MASTER THESIS

TOWARDS REAL-TIME ESTIMATION OF GROUND REACTION FORCES USING 3 IMUS

Carol Robert Derla

FACULTY OF ENGINEERING TECHNOLOGY
DEPARTMENT OF BIOMECHANICAL ENGINEERING

EXAMINATION COMMITTEE
prof.dr.ir. Massimo Sartori
dr.ir. Mohamed Irfan Refai
Ing. Donatella Simonetti MSc
Ing. Junhao Zhang MEng

DOCUMENT NUMBER
BE - 954

UNIVERSITY OF TWENTE.

19-09-2023

Towards Real-Time Estimation of Ground Reaction Forces using 3 IMUs

Carol R. Derla
BME Master, Medical Device Design Track, University of Twente, Enschede, Netherlands

Abstract

In biomechanical analysis, accurately estimating Ground Reaction Forces (GRFs) is crucial. Conventionally, this requires expensive force plates (FP) and complex gait laboratories. Our study explores the feasibility of estimating GRFs using a simplified setup of only three Inertial Measurement Units (IMUs): one placed on the pelvis and one on each foot. We investigated the accuracy of GRFs estimation at three different walking speeds (0.28m/s, 0.83m/s, 1.39m/s) for both feet. To make this possible, our method applies the Constant Walking Speed Assumption (CWSA) to investigate the real-time implementation of the Smooth Transition Assumption (STA). Although our approach encounters challenges with the accuracy of GRFs estimation at lower speeds and with the estimation of shear forces, potential solutions such as advanced signal processing, and the use of force-sensitive resistors (FSRs) could offer mitigation strategies. This research contributes to the field of biomechanics by suggesting a cost-effective and simplified method for estimating GRFs, with potential applications in sports science, clinical rehabilitation, and the design of assistive devices for individuals with mobility impairments.

Keywords: Ground Reaction Forces, Gait Analysis, Inertial Measurement Units, Smooth Transition Assumption, Biomechanics.

1. Introduction

Assessing walking capacity and gait rehabilitation is of utmost importance in clinical practice or sport biomechanics. It enables clinicians to diagnose and monitor patients' progress, evaluate the effectiveness of interventions, and design personalized rehabilitation plans. Ground reaction forces (GRFs) during walking are a critical measure for assessing motor deficits [1], providing valuable information about gait pattern, balance, and muscular strength [2] [3].

Traditional methods of measuring ground reaction forces (GRFs) during walking, use force plates [4] instrumented in treadmill or embedded in the floor [5]. However, it is important to note that these methods may not fully capture the complexity of real-life gait situations, potentially affecting the validity of the assessment [6].

An alternative solution in the form of wearable technology: pressure insoles, embedded within the user's shoes, provide real-time data on the distribution of forces exerted on the feet during various activities [2]. The most significant advantage of pressure insoles is their ability to offer a non-intrusive and portable method for collecting data [7], while capturing detailed spatial and temporal pressure patterns, allowing for a comprehensive analysis of foot dynamics. However, pressure insoles have their limitations. They only focus on measuring plantar pressure and cannot provide insight into other aspects of kinematic data such as body motion and posture. Thus, they can't function as a stand-alone system for biomechanical gait analysis and must be paired with a kinematic capture system such as a motion capture system or inertial measurement units (IMUs).

By replacing the current gold-standard set-up, which typically involves a motion capture system and force plates, with only three IMUs, we can realize several advantages [8]. Firstly, IMUs are wearable and do not require a specific walking area, allowing for more natural and realistic gait assessment. Secondly, IMUs are affordable, making them accessible to outpatient clinics and home-based rehabilitation. Lastly, due to a non-restrictive walking area and user-friendliness, the IMU system could potentially promote continuity of care and reduce the need for frequent clinic visits, consequently improving rehabilitation plan adherence. Therefore, the ability to estimate GRFs using only three IMUs offers a less invasive, more cost-effective, and flexible solution for monitoring motor deficits during rehabilitation. IMUs are small sensors that can measure accelerations, angular velocities, and orientations of body segments [9]. These devices provide a less invasive and flexible means of obtaining kinematics data during any type of movement. In this paper, we estimate GRFs during walking tasks.

Several studies have explored the use of IMUs for GRFs estimation. However, most of these studies have relied on multiple sensors, increasing both the cost and complexity of the setup [9,10,11,12,13]. This multi-sensor configuration not only introduces calibration challenges but also often requires a less straightforward learning curve for clinicians and introduces more limitations to the patients movement [14]. Moreover, a significant characteristic of these existing state of the art methodologies is that they are largely designed for offline data processing. In other words, the conventional approach involves conducting the walking or running experiment, collecting the data, and then post-processing it offline to estimate GRFs. This lack of real-time analysis restricts its utility in immediate clinical decision-making or real-time performance adjustments in sports settings.

Our research, in contrast, aims to simplify the GRFs estimation process by using only three IMUs strategically placed on the pelvis and both feet as seen in as seen in **Figure 2**. Our methodology is designed to use data up to the investigated point, effectively simulating real-time usage of the system.

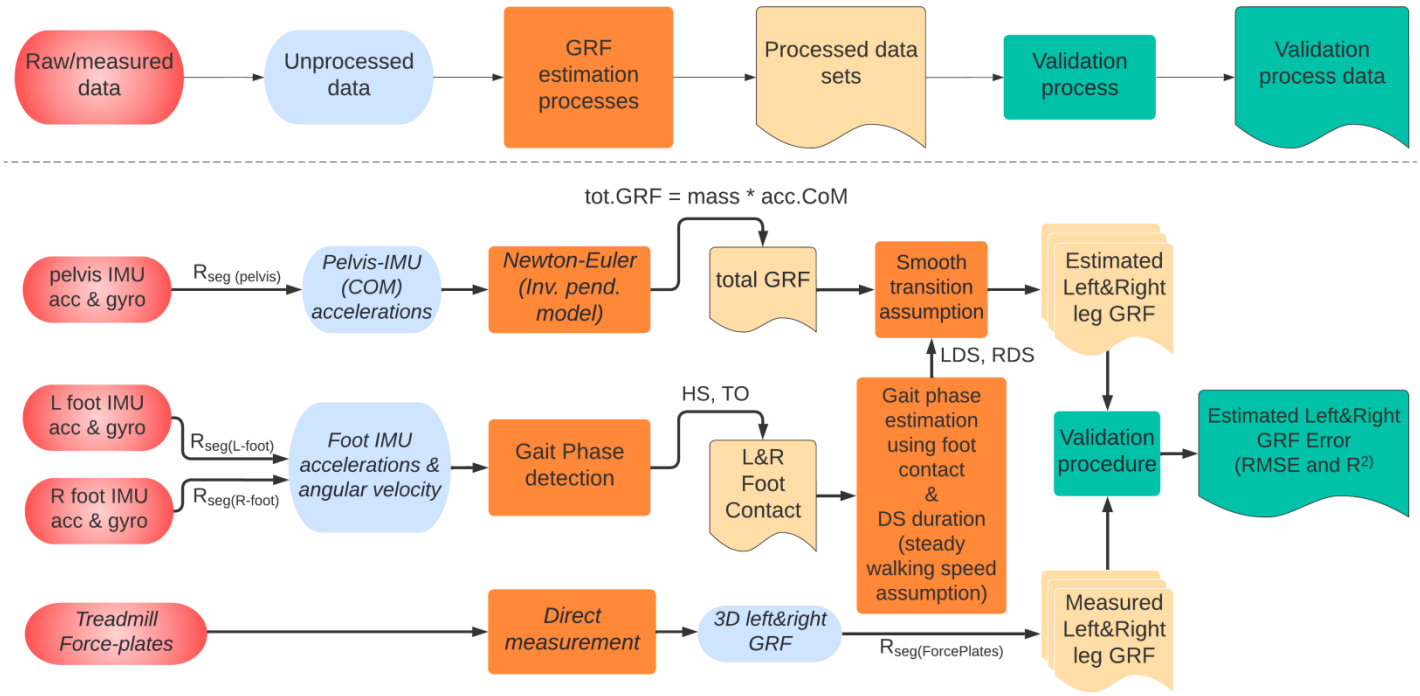

Figure 1: System flowchart. The flowchart represents the data processing flow. From left to right: IMU and FP data calibration procedure, total GRF estimation, and gait phase detection followed by STA and validation procedure. On top, there are presented the blocks' color and geometrical code.

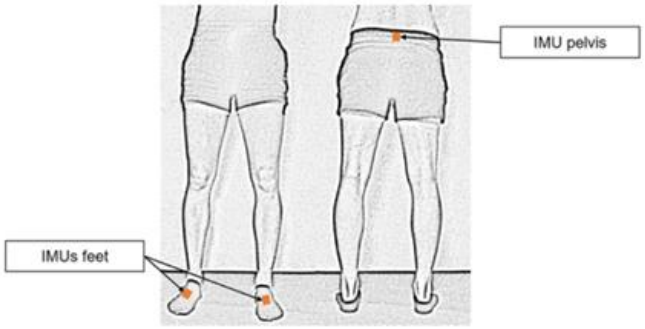

Figure 2: The placement of the three IMUs: one on the lower back, one on the left foot, and another one on the right foot. The picture has been adapted from the following source [15].

Our research aims to develop a method for accurately estimating left and right leg GRFs during walking using a minimal number of wearable sensors. We investigate the feasibility of using three IMUs: one on the pelvis to measure the total GRF, one on the left foot, and one on the right foot to detect gait phases in order to split the total GRF into the left and right foot GRFs as presented in **Figure 1**. We focus on determining whether these three IMUs are sufficient for accurate GRFs estimation.

The following sections present our assumptions, hypothesis, and methodology for estimating GRFs using three IMUs. We also provide details about the conducted experiment, discuss the obtained results and the evaluation of our method's accuracy. Finally, we address the limitations of our approach and suggest areas for future research.

2. Methods

This section describes the approach taken to estimate GRFs during walking using IMUs and to validate the accuracy of the estimation. The method involved sensor calibration, estimation of total GRF, gait phase detection using foot contact events, and splitting the total GRF into left and right foot GRFs (see **Figure 2**). An experimental setup was implemented, and data collection and processing were performed. The validation procedure consisted of two tests to assess the agreement in amplitude and shape between the estimated and measured GRFs for each foot in 3D. This structured approach and validation procedure ensured a comprehensive analysis of the GRF estimation and its accuracy during walking.

2.1. IMU Calibration

A sensor-to-segment calibration technique described by Bonnet et al. [16] was used. A calibration process is required to transform the measurements from sensor reference to pelvis segment reference frame, enabling relevant analysis of gait kinematics using IMUs [17]. The pelvis segment reference frame coordinates are as follows: X-axis is the antero-posterior axis of the pelvis, Y-axis is the medio-lateral axis of the pelvis and Z-axis is the vertical axis of the pelvis. The calibration procedure involved the following:

Step 1: During an initial standing still position, the orientation estimate, vertical Z-axis (ax_Z), for all segments was obtained from the 3D accelerometer data y_A^s,, which measures only gravitational acceleration (1a).

$$ax_Z = \frac{y_A^s}{||y_A^s||} \quad (1a)$$

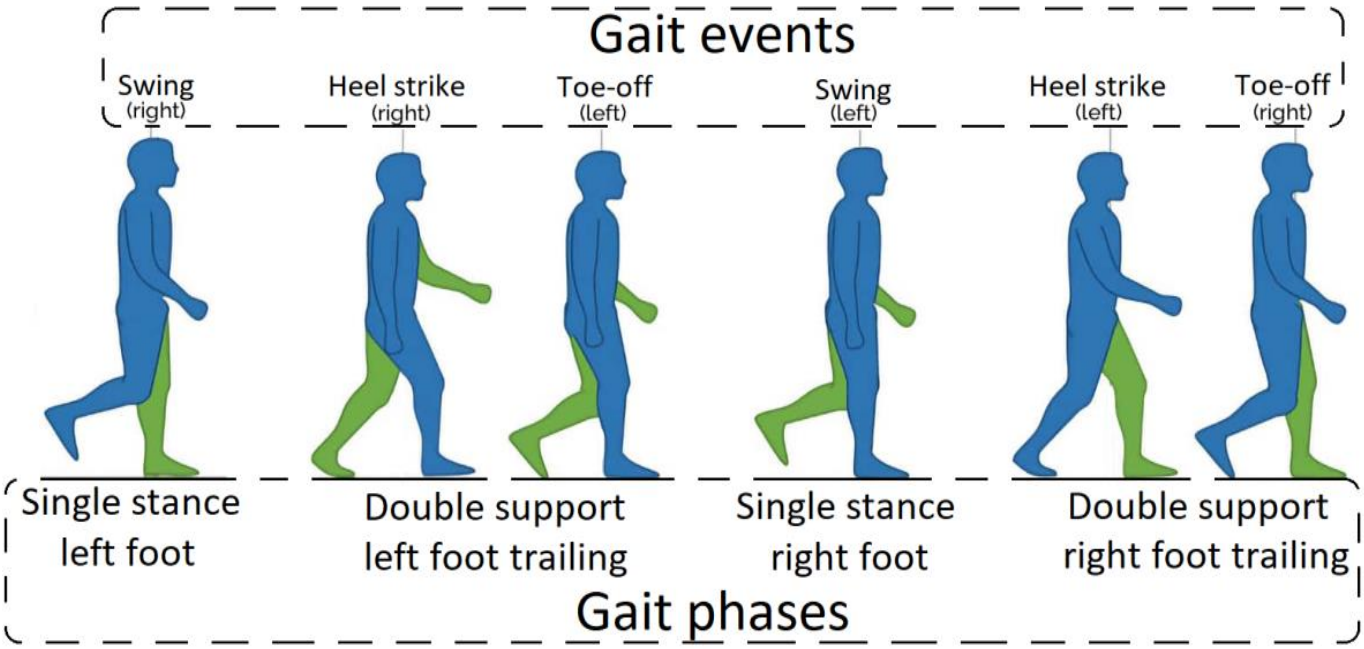

Figure 3: The figure represents the division of the gait cycle. On the bottom are the four gait phases: Single stance left foot, Double support left foot trailing, Single stance right foot, and Double support right foot trailing. On top are the gait events that dictate the transition between the respective phases. The picture has been adapted from the following source [18].

Step 2: The orientation of Y-axis (ax_Y) of the pelvis was estimated by asking the subject to bend forward. The axis measuring the largest angular rotation was found using principal component analysis (PCA) (1b), on the gyroscope output y_G^s,

$$ax_Y = PCA(y_G^s) \quad (1b)$$

which was then used to estimate the orientation of the X-axis (ax_X) of the pelvis (1c).

$$ax_X = ax_Y \times ax_Z \quad (1c)$$

Step 3: The orientation of Y-axis was updated using the right-hand thumb rule (1d) in order to keep X, Y and Z orthogonal.

$$ax_Y = ax_Z \times ax_X \quad (1d)$$

$$R_{seg(IMU)} = [\, ax_X \; ax_Y \; ax_Z \,] \quad (1e)$$

The sensor-to-segment calibration was represented by the rotation matrix R_{seg} (1e), where ax_X, ax_Y and ax_Z are the orthogonal unit vectors defining the local coordinate system of the segment with respect to the sensor.

The foot IMUs are calibrated with the same method of sensor-to-segment calibration technique. This transforms the sensor reference to a foot segment reference frame, where X-axis is the toe-heel axis, Y-axis is the lateral-medial axis and Z is the vertical axis.

Instead of a bending trial, a short walking trial was performed in order to compute the ax_Y of the feet IMU. Thus, the orientation of Y-axis of each of the feet IMUs was estimated, using equation (1b), as the axis measuring the largest angular rotation, mainly due to plantar flexion and dorsiflexion.

The FP data were also rotated 90° around the Z axis, in order to flip the XY plane so X becomes the walking direction and Y medio-lateral, through $R_{seg(ForcePlates)}$ (1f).

$$R_{seg(ForcePlates)} = \begin{bmatrix} 0 & -1 & 0 \\ 1 & 0 & 0 \\ 0 & 0 & 1 \end{bmatrix} \quad (1f)$$

2.2. Estimating Total GRF

The biomechanical assumption that the center of mass (CoM) is contained within the rigid pelvis is widely used to estimate the instantaneous 3D total GRF using a single IMU during gait [17]. Therefore, an IMU at the pelvis can measure the CoM accelerations. Using Newton's second law (2a), the product of body mass and CoM accelerations, we calculate the whole body GRF, as in the following equation:

$$GRF = m \cdot acc_{CoM} \quad (2a),$$

where GRF is the 3D total GRF, m is the subject's mass, and acc_{CoM} represents the accelerations in 3D of the subject's center of mass. Formula (2a) is presented in **Figure 2** as well as the process of Newton-Euler (Inv. pend. model). It is assumed that the feet are the only contact with the external world, and no additional load is carried by the body. This assumption allows us to focus on the dynamics of the center of mass during gait, considering the inverted pendulum model.

2.3. Gait phase detection using Foot Contact Detection - Heel Strike (HS) and Toe Off (TO) Detection

The gait cycle was divided into four phases: as seen in **Figure 3**. Each gait event (HS right, TO left, HS left, TO right) updates the respective phase of the gait cycle. For instance, when HS right is detected, the algorithm transitions from the double support right foot trailing phase to the single stance right phase. Similarly, when TO left is detected, the algorithm transitions from the single stance left phase to the double support left foot trailing phase. This information is needed for splitting the total 3D GRF into left and right foot GRFs. To detect the gait phases, the algorithm considers the detected gait events (HS and TO) from both the left and right foot.

Following the system flowchart from **Figure 2**, HS and TO events were detected using accelerometer and gyroscope data obtained from the IMUs placed on the feet. The proposed algorithm for HS detection used antero-posterior (X) and vertical (Z) linear accelerations, as well as mediol-ateral (Y) angular accelerations. For TO detection, antero-posterior (X) and vertical (Z) linear accelerations, as well as medio-lateral (Y) and vertical (Z) angular accelerations were used.

The approach was developed through a trial and error process, where different thresholds were tested and adjusted until a suitable formula was found. To ensure robustness across trials, the detected instances were compared with the instances detected from the force plates. The thresholds used in the algorithm were automatically computed based on the mean and standard deviation of the accelerometer or gyroscope data obtained during the calibration walking trial. This iterative process helped refine the approach and ensure its effectiveness in accurately detecting the events of interest. The thresholds used for HS and TO detection can be seen in **Table 1**.

Table 1: HS and TO thresholds

HS threshold	X_{acc}	$(mean(X_{acc}) + std(X_{acc})) \cdot 2$
	Z_{acc}	$mean(Z_{acc}) + std(Z_{acc})$
	Y_{gyro}	$std(Y_{gyro}) + 1$
TO threshold	X_{acc}	$\frac{\text{std}(X_{acc})}{\text{mean}(X_{acc})} - 1$
	Z_{acc}	$mean(Z_{acc})$
	Y_{gyro}	$std(Y_{gyro}) \cdot (-1) + 1$
	Z_{gyro}	$mean(Z_{gyro})$

Where, X_{acc} refers to the X-axis accelerometer measurements, which represent the acceleration value in the antero-posterior (X) direction. Z_{acc}, represents the Z-axis accelerometer measurements, indicating the acceleration value in the vertical direction (Z). Y_{gyro} and Z_{gyro} correspond to the Y-axis and Z-axis gyroscope measurements, capturing the angular velocity around the Y-axis and Z-axis.

2.4. Split total GRF into left and right foot GRF – (Smooth Transition Assumption & Constant Walking Speed Assumption)

The total 3D GRF is split into left and right foot GRFs using the Smooth Transition Assumption (STA). The system flowchart from **Figure 2** shows that STA uses the previously determined four gait phases and the Constant Walking Speed Assumption (CWSA). The left and right foot GRFs are estimated based on the timing and sequence of the HS and TO events detected from the IMUs on the left and right feet.

The total GRF was split in left and right GRFs assuming that the load is smoothly transferred from one foot to the other during double stance support and was modeled as an exponential function dependent on the duration of the double support phase [10]. The vertical and medio-lateral STA is computed using the formula (3a).

$$f_{v\&m\text{-}STA} = e^{(-(t/Tds)^3)} \quad (3a),$$

where t is the time elapsed during the double support phase, and T_{ds} is half the duration of the double support phase [10].

The anterio-posterior STA function is computed using the formula (3b).

$$f_{ap\text{-}STA}=(k_1 \cdot e^{-\left[\frac{t-t_p}{T_{ds}}\right]^2} - \frac{k_2 t}{T_{ds}}) \quad (3b),$$

where $t_p = \frac{2T_{ds}}{3}$ and the constants are $k_1 = e^{4/9}$ and $k_2 = k_1/2 \cdot e^{-16/9}$ [10].

The CWSA assumes a constant walking speed of the subject during data collection and therefore a constant double support phase throughout the entire walking task.

2.6. Experimental setup

Participants performed various walking tasks on a treadmill equipped with force plates while wearing IMUs on their pelvis and feet, along with markers for a motion capture system. All tasks were recorded twice.

The experiment began by having participants stand still with their feet shoulder-width apart in the middle of the treadmill for 10 seconds. Participants were then instructed to bend forward and return to their static position, in a 10 seconds interval. Additionally, during the calibration trial, participants were asked to walk for 10 seconds to calibrate the foot IMUs.

Following the calibration phase, participants were asked to perform different walking tasks on the treadmill:

1) Walk at 0.28m/s: Participants walked on a treadmill at a speed of 0.28m/s for 30 seconds.

2) Walk at 0.83m/s: Participants walked on a treadmill at a speed of 0.83m/s for 30 seconds.

3) Walk at1.39m/s: Participants walked on a treadmill at a speed of 1.39m/s for 30 seconds.

Throughout the experiment, participants were given time to familiarize themselves with the treadmill before starting the recording.

2.7. Data collection and processing

An instrumented treadmill (M-Gait, MotekForce Link, Netherlands, 1000 Hz) captured 3D GRFs. The 3D kinematics were obtained using both an inertial motion capture system (100 Hz, MVN Link, Xsens, Enschede, the Netherlands) and an eight-camera optical motion capture system (Qualisys Oqus, Göteborg, Sweden). The inertial motion capture system consisted of three IMUs placed on the participants: one at the pelvis (L5) and one on each foot. The IMUs were securely attached using neoprene Velcro bands. The IMUs collected 3D linear accelerations and 3D angular velocities.

Reflective markers, following the Plug-in Gait lower-body marker model [19], were placed on the participants, totaling 18 markers (128 Hz).

Using a BNC cable, the motion capture system and IMU system were automatically synchronized. The pulse sent through the BNC cable was used to automatically initiate the IMU recording when the Qualisys recording was initiated from the software. The synchronizer ensured the proper synchronization of data recordings.

The collected data were then processed in MATLAB® 2018b (Mathworks, Natick, Massachusetts, USA). The acceleration and gyroscope data were filtered using a zero-phase low-pass Butterworth filter with a cutoff frequency of 5 Hz in the vertical direction and 4 Hz in the antero-posterior and medio-lateral directions to reduce high-frequency noise. The estimated left and right GRF was computed using the algorithm described earlier, sections *2.2* and *2.4*.

The force plate-recorded GRFs were filtered with the same cutoff frequency as the IMU data to avoid phase shift.

2.8. Validation procedure

Two tests were conducted to evaluate the accuracy of the algorithm. The statistical analysis investigated the similarity in amplitude and shape between the measured experimental and estimated GRFs using the three IMUs.

Both tests were performed separately for the left and right foot GRFs in all three directions. All data analysis was performed in MATLAB® 2018b (Mathworks, Natick, Massachusetts, USA).

Test 1 aimed to evaluate the agreement between the estimated and measured GRFs in all three directions for each foot. The root mean square error ($RMSE$) (4a), which is a metric that tells how far apart the predicted values are from the observed values in a dataset, on average, was calculated across the full gait gait cycle [19].

$$RMSE = \sqrt{\frac{\sum_{i=1}^{N}(y_i - x_i)^2}{N}} \quad (4a),$$

where x is the GRF reference and y is the estimated GRF, $\bar{x}$ is the mean of the GRF measurement. Lastly, N is the number of data points. Same notation was used for Test 2 in (4b).

Test 2 focused on assessing the similarity in shape between the estimated and measured GRFs. The coefficient of determination (R^2) (4b), was used to measure the proportion of variance explained by the estimator model. This provides a measure of the agreement in waveform characteristics between the estimated and measured GRFs [20].

$$R^2 = 1 - \frac{\sum_i^N (x_i - y_i)^2}{\sum_i^N (x_i - \bar{x})^2} \quad (4b)$$

Furthermore, the significance of the correlation was determined using a two-tailed hypothesis t test [21] with a significance level (p-value) of 0.05.

3. Results

Table 3 presents the errors in estimating the 3D GRFs over the complete gait trial. The $RMSE$ % Body Weight values displayed in the table are the left and right foot for all subjects, all walking speeds and all directions X, Y and Z. Moreover, the mean and standard deviation (±std) across all subjects for each speed are presented on the bottom.

For the left foot, the mean $RMSE$ (%BW) for all subjects walking at 0.28m/s were 2.12±0.44%, 2.27±0.51% and 10.74±1.9% for X, Y and Z, respectively. At a walking speed of 0.83m/s, the errors increased to 5.37±2.12%, 5.44±2.50% and 11.98±1.29% for X, Y and Z, respectively. When the walking speed was further raised to 1.39 m/s, the errors were 8.04±2.33%, 6.02±1.72% and 13.67±1.24% X, Y and Z, respectively.

For the right foot, the mean $RMSE$ for all subjects walking at 0.28m/s were 2.71±0.76%, 2.32±1.04%, and 10.55±1.65% for X, Y and Z axes, respectively. When the walking speed was increased to 0.83m/s, the RMS errors rose to 6.33±3.12%, 4.27±2.20%, and 14.15±1.32% for X, Y and Z, respectively. Finally, at the highest tested walking speed of 1.39m/s, the RMS errors were 7.19±1.65%, 5.73±1.48%, and 12.50±2.33% for X, Y and Z.

Table 4 presents the R^2 values in estimating the 3D GRFs over the entire gait trial. The R^2 values included in the table represent both the left and right foot for all subjects, across varying walking speeds and in all directions X, Y and Z. The mean R^2 values across all subjects for each direction and speed are presented at the bottom of the table.

For the left foot, at a walking speed of 0.28m/s, the R^2 mean values across all subjects were 0.14±0.04, 0.40±0.22, and 0.74±0.02 for X, Y and Z axes respectively. When the walking speed was increased to 0.83m/s, the R^2 values changed to 0.32±0.13, 0.23±0.11, and 0.82±0.06 for X, Y and Z. At the maximum tested speed of 1.39m/s, the R^2 values were 0.31±0.08, 0.32±0.16, and 0.90±0.02 for X, Y and Z.

For the right foot, at a walking speed of 0.28m/s, the R^2 values were 0.25±0.21, 0.38±0.24, and 0.75±0.01 for X, Y and Z. As the walking speed was increased to 0.83m/s, the R^2 values were 0.36±0.15, 0.19±0.08, and 0.87±0.04 for X, Y

and Z. Finally, at a speed of 1.39m/s, the R^2 values were 0.28±0.1, 0.28±0.15, and 0.90±0.02 for X, Y and Z.

Figure 4 provides a visual representation of the IMU estimated GRF (solid lines) and FP measured GRF (dotted lines) for the left and right foot in 3D. In the vertical - Z dimension, the estimated GRFs show a good match, although with slight overshoot observed at points of inflection in relation to the measured GRF. The antero-posterior - X direction exhibits a fair match, as evidenced by the similar profiles observed in the plot. However, in the medio-lateral - Y direction, the level of similarity is less precise, with the estimated and measured GRFs displaying little overlap. The error between the FP and IMU estimated GRFs is visually depicted, under each plot for each axis, in the form of a blue line.

Table 3: Comparing the Estimated and Reference GRF values: Root Mean Square Error ($RMSE$) expressed in % body weight.

	Left foot								
	Walk at 0.28m/s			**Walk at 0.83m/s**			**Walk at 1.39m/s**		
	X	Y	Z	X	Y	Z	X	Y	Z
subj 1	2.93	2.60	10.72	4.76	3.93	11.49	6.49	5.54	11.44
subj 2	2.02	1.64	10.36	7.16	8.06	12.16	9.00	7.92	13.81
subj 3	1.60	2.59	11.94	5.41	3.71	12.21	8.44	4.02	13.88
subj 4	2.10	2.07	9.60	8.93	9.16	9.91	12.72	7.50	15.57
subj 5	1.84	2.33	8.09	2.35	3.29	13.72	6.18	7.75	13.12
subj 6	2.45	3.00	14.15	4.73	6.76	11.12	6.32	5.51	13.66
subj 7	1.93	1.64	10.34	4.27	3.17	13.24	7.16	3.89	14.18
Mean ±std	2.12 ±0.44	2.27±0.51	10.74±1.9	5.37±2.1	5.44±2.5	11.98±1.29	8.04±2.33	6.02±1.72	13.67±1.24
	Right foot								
	Walk at 0.28m/s			**Walk at 0.83m/s**			**Walk at 1.39m/s**		
	X	Y	Z	X	Y	Z	X	Y	Z
subj 1	3.23	2.61	10.22	4.32	3.60	12.16	6.04	6.16	9.96
subj 2	1.59	1.87	10.46	7.93	5.94	12.77	9.02	5.80	13.48
subj 3	3.54	1.61	11.9	1.17	0.89	14.94	7.38	4.18	9.83
subj 4	3.16	2.39	9.57	10	7.48	14.52	9.65	7.03	15.75
subj 5	2.09	1.87	7.99	6.43	4.81	15.68	5.24	7.55	10.73
subj 6	3.28	4.49	13.18	9.50	4.80	15.27	5.89	5.98	13.41
subj 7	2.12	1.43	10.50	5.00	2.38	13.74	7.10	3.38	14.36
Mean ±std	2.71±0.76	2.32±1.04	10.55±1.65	6.33±3.12	4.27±2.2	14.15±1.32	7.19±1.65	5.73±1.48	12.5±2.33

Table 4: Comparing the Estimated and Reference GRF values: Coefficient of determination (R^2). $^*p < 0.05$**.** The color code of the table was chosen empirically just for better visualization of the table as such: Green for very good values (R^2 or > 0.8), Orange for acceptable values ($0.6 < R^2 < 0.8$) and Red for not good estimation ($R^2 < 0.6$).

	Left foot								
	Walk at 0.28m/s			**Walk at 0.83m/s**			**Walk at 1.39m/s**		
	X	Y	Z	X	Y	Z	X	Y	Z
subj 1	0.14*	0.16*	0.75*	0.41*	0.15*	0.84*	0.33*	0.18*	0.90*
subj 2	0.10*	0.55*	0.75*	0.53*	0.14*	0.83*	0.35*	0.50*	0.91*
subj 3	0.21*	0.10*	0.73*	0.21*	0.36*	0.71*	0.20*	0.16*	0.92*
subj 4	0.10*	0.58*	0.76*	0.17*	0.18*	0.82*	0.39*	0.36*	0.86*
subj 5	0.12*	0.57*	0.75*	0.38*	0.15*	0.88*	0.19*	0.31*	0.91*
subj 6	0.11*	0.29*	0.71*	0.30*	0.23*	0.88*	0.38*	0.54*	0.89*
subj 7	0.19*	0.57*	0.75*	0.23*	0.41*	0.82*	0.30*	0.17*	0.92*
Mean(±std)	0.14±0.04*	0.40±0.22*	0.74±0.02*	0.32±0.13*	0.23±0.11*	0.82±0.06*	0.31±0.08*	0.32±0.16*	0.90±0.02*
	Right foot								
	Walk at 0.28m/s			**Walk at 0.83m/s**			**Walk at 1.39m/s**		
	X	Y	Z	X	Y	Z	X	Y	Z
subj 1	0.29*	0.12*	0.75*	0.46*	0.16*	0.83*	0.37*	0.15*	0.91*
subj 2	0.38*	0.30*	0.75*	0.57*	0.13*	0.93*	0.35*	0.45*	0.92*
subj 3	0.64*	0.09*	0.73*	0.37*	0.28*	0.81*	0.14*	0.14*	0.92*
subj 4	0.13*	0.64*	0.76*	0.15*	0.13*	0.85*	0.42*	0.37*	0.86*
subj 5	0.11*	0.53*	0.77*	0.42*	0.13*	0.88*	0.19*	0.13*	0.91*
subj 6	0.09*	0.31*	0.72*	0.36*	0.15*	0.89*	0.22*	0.49*	0.90*
subj 7	0.09*	0.66*	0.75*	0.19*	0.33*	0.91*	0.26*	0.25*	0.91*
Mean(±std)	0.25±0.21*	0.38±0.24*	0.75±0.01*	0.36±0.15*	0.19±0.08*	0.87±0.04*	0.28±0.10*	0.28±0.15*	0.90±0.02*

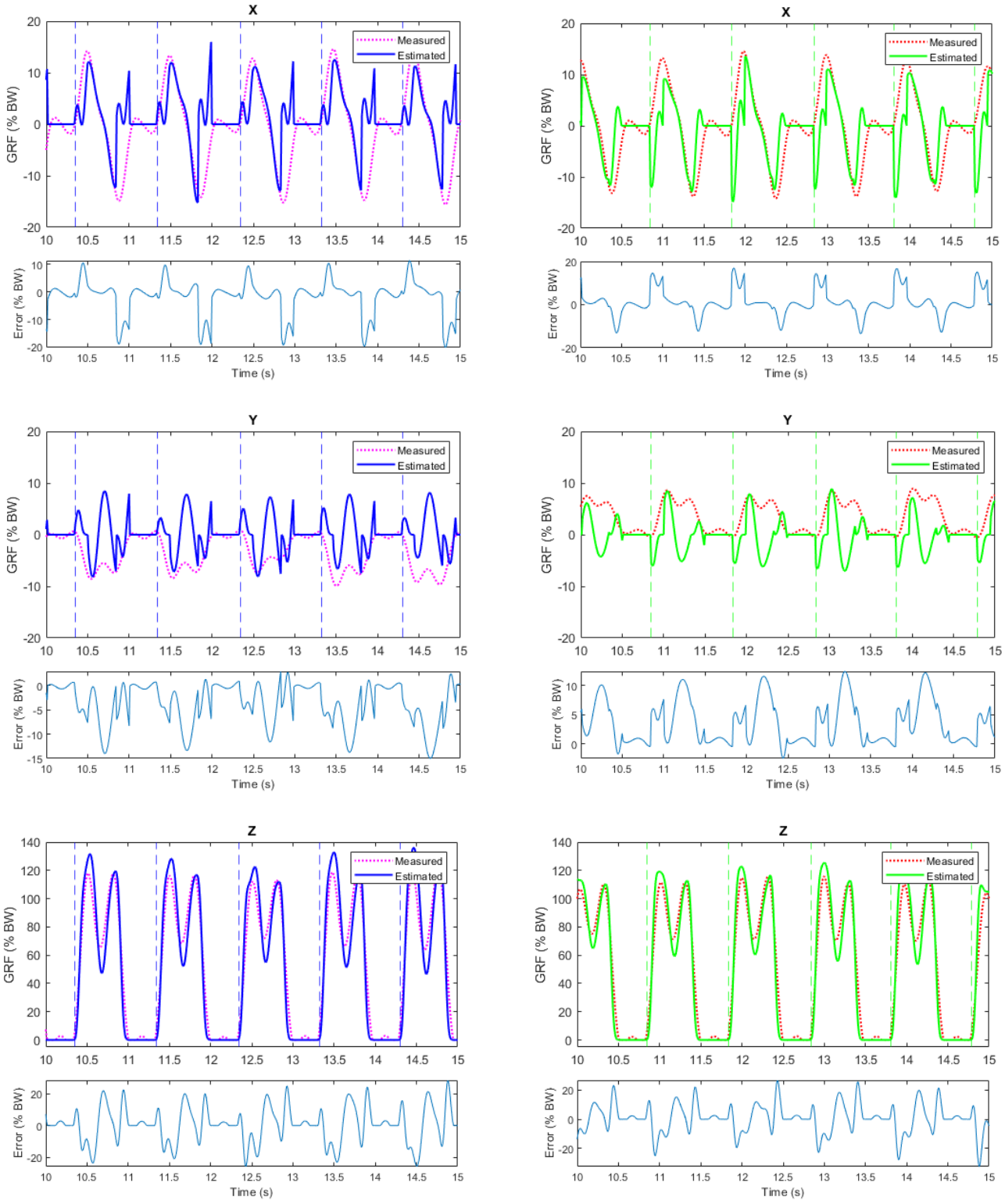

Figure 4: Snapshot of the 3D FP measured (dotted lines) and IMU estimated (solid lines) GRF for left and right foot for the 1.39m/s walking speed trial. The top figures are the X axis, in the middle are the Y axis and on bottom are the Z axis. The vertical dotted lines (blue for left foot and green for right foot) represent heel strike instances. Underneath each plot, with blue line are the error difference between the measured and estimated GRF.

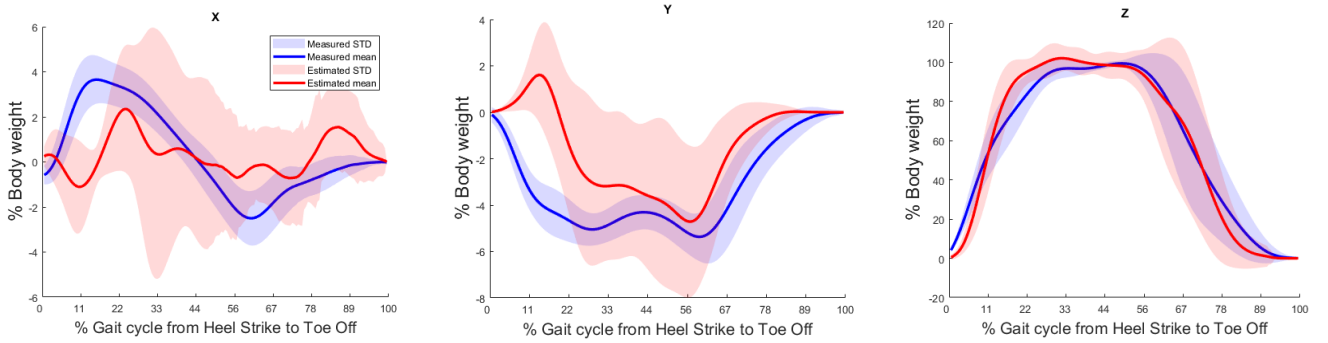

Figure 5: The figure represents the FP measured and IMU estimated GRF mean and standard deviation as shaded for the left foot across all subjects as % of the gait cycle for the 0.28m/s walking speed

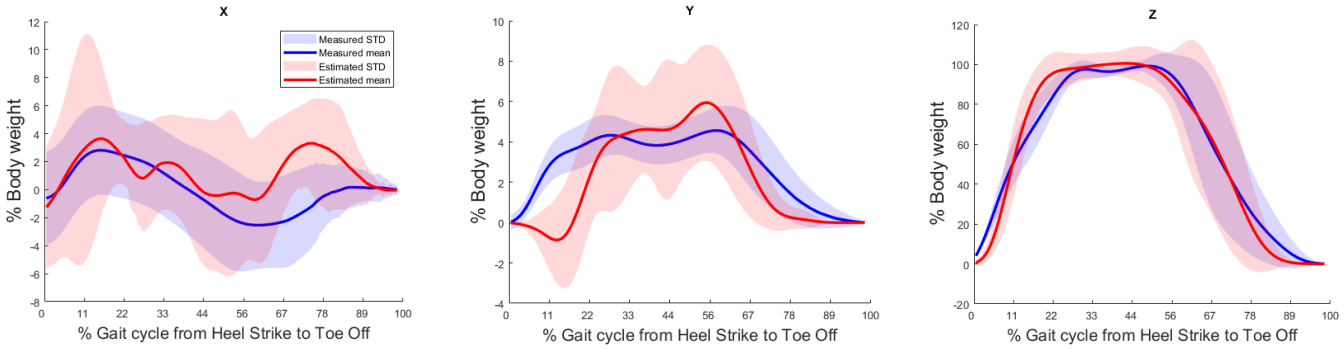

Figure 6: The figure represents the FP measured and IMU estimated GRF mean and standard deviation as shaded for the right foot across all subjects as % of the gait cycle for the 0.28m/s walking speed

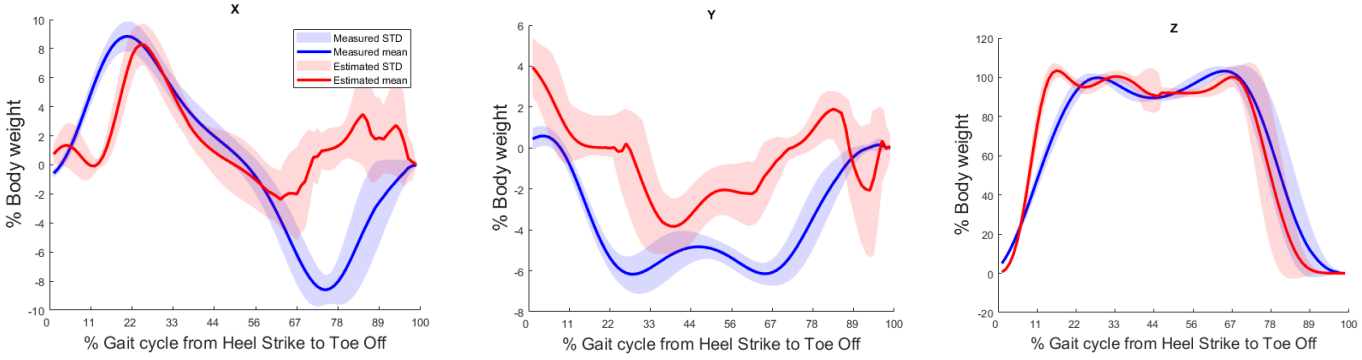

Figure 7: The figure represents the FP measured and IMU estimated GRF mean and standard deviation as shaded for the left foot across all subjects as % of the gait cycle for the 0.83m/s walking speed

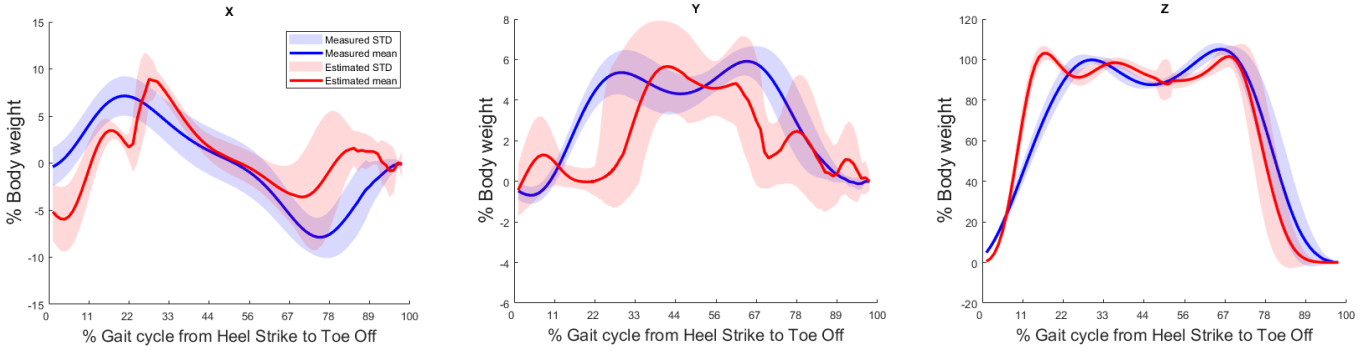

Figure 8: The figure represents the FP measured and IMU estimated GRF mean and standard deviation as shaded for right foot across all subjects as % of the gait cycle for the 0.83m/s walking speed

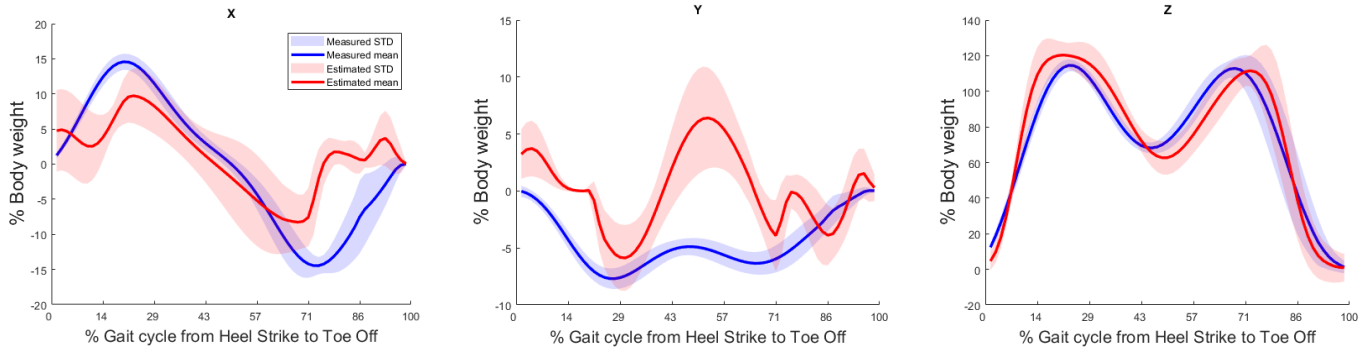

Figure 9: The figure represents the FP measured and IMU estimated GRF mean and standard deviation as shaded for left foot across all subjects as % of the gait cycle for the 1.39m/s walking speed

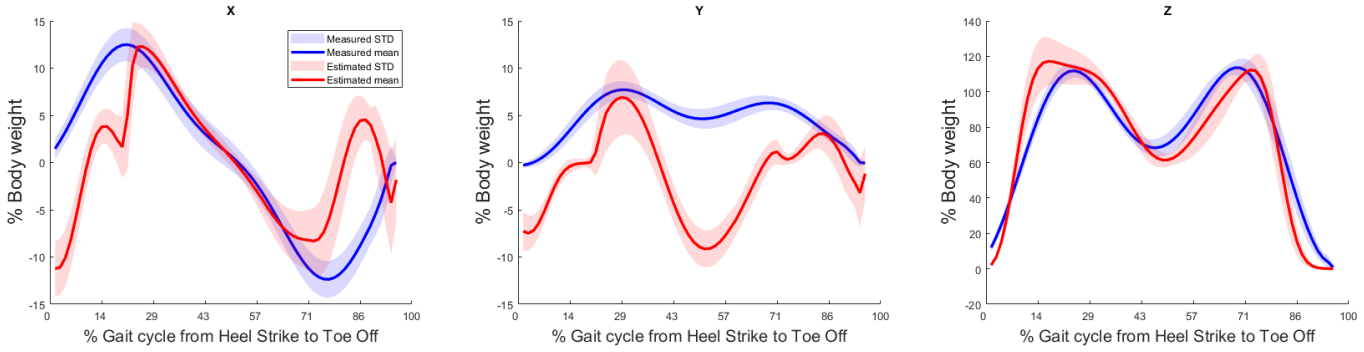

Figure 10: The figure represents the FP measured and IMU estimated GRF mean and standard deviation as shaded for right foot across all subjects as % of the gait cycle for the 1.39m/s walking speed

The error is oscillating between -20% and +20% to 0% and 0% to +15% in the medio-lateral and -15% to +15% for the anterior posterior.

Figures 5 to **10** present the mean and standard deviation (represented as the shaded area) of the GRFs for the left and right foot at different walking speeds (0.28m/s, 0.83m/s, and 1.39m/s), respectively. Each figure is divided into three plots corresponding to the X, Y, and Z components of the GRF. For the 0.28m/s it can be seen the biggest variation as the shaded graph has the biggest area of all, especially for shear forces. There is a better correlation between estimated and measured forces in all three directions for 0.83m/s, even if the variation is still bigger than for 1.39m/s. And for 1.39m/s we observed the smallest variation in shear forces and the highest correlation for vertical and posterior-anterior forces, but for the latero-medial plots, the bigger accelerations result in a lower correlation as the 40% to 60% region significantly deviates from the true GRF.

4. Discussion

Our research aimed to innovate in the field by investigating the feasibility of estimating left and right foot GRFs through a simple setup of three IMUs placed as such: one IMU on the pelvis for total GRF assessment and one IMU each on the left and right foot for detecting gait phases. Although the estimations weren't conducted in real-time during the experiment, where we solely collected IMU and FP data, the uniqueness of our approach lies in its exploration of potential real-time applications. The feasibility of real-time GRF estimation emerges from our methodology, which utilizes processes that consider data only up to the currently estimated instance. This included the application of the CWSA for STA implementation and avoiding post-processing. For the successful application of STA, it's necessary to have initial knowledge of the double stance duration [10]. However, our approach bypasses this requirement through the use of CWSA, by assuming constant walking speed STA used a subject-specific predefined duration, computed during a short walking calibration trial, for all double stance GRF estimations during the trial. This strategy aimed to decrease both the expense and complexity related to experimental GRF measurement.

Our findings from GRF estimations show that the accuracy of the estimation increased in variability as walking speeds rose. The $RMSE$ values from **Table 3**, when measured for both feet at different speeds (0.28m/s, 0.83m/s, and 1.39m/s), exhibited a clear trend of increasing variability as the speed of walking increased. This increase in variability can be attributed to the higher accelerations resulting in higher reaction forces, present at increased speeds. At higher walking speeds, the forces acting on the body increase, which in turn leads to greater variability in the GRFs, causing the estimation accuracy to be more inconsistent. As a result, the $RMSE$ (%BW) becomes larger.

Thus, the increase in variability in the accuracy of GRF estimations with higher walking speeds is a significant finding that could have implications for the future design and

application of IMU-based GRF estimation systems. Given this variability, it could be beneficial to create systems equipped with more advanced filtering or signal processing techniques.

Despite the increased variability in accuracy with higher walking speeds, a trend can be identified where the correlation between the estimated and actual GRFs actually increases with speed. Looking at the R^2 results, it becomes apparent that with increasing walking speeds, the correlation coefficients consistently show an upward trend, implying an enhanced estimation accuracy despite the larger variability.

The correlation increases with speed, demonstrating that estimating GRF at lower speeds is more challenging [17]. This challenge could arise due to the lower contact forces and smaller accelerations at slower speeds, which can make it more difficult to estimate the more nuanced dynamics. In other words, slower speeds might present less distinct patterns, making the estimation task more complex.

The results obtained from our research, mainly the correlation coefficients R^2 from **Table 4**, demonstrate lower values for shear forces compared to vertical forces. **Figure 4**, further corroborates these findings, depicting higher discrepancies for estimated shear force. This is suggestive of a weaker relationship between actual and estimated shear forces, thus, estimating shear GRF using IMUs is the most challenging aspect [14]. This is mainly because the position of the IMU on the human body significantly influences the accuracy of the measurements. Since the IMUs were affixed to the body's center of mass (the pelvis), accurately capturing shear forces, which are inherently distributed and variable across the foot-ground interface [22], was a challenge. Further post-processing for removing impact impulse, or soft tissue artifacts is necessary for improved R^2.

Compared to the models developed by Ren et al. and Karatsidis et al., our study showed varying degrees of correlation in different components. In the vertical component, our model demonstrated comparable performance, with an R^2 value of 0.9, matching the R^2 value of 0.9 reported in both Ren et al. [10] and Karatsidis et al. [11]. However, our study lagged in the anterior and lateral planes, recording R^2 values of 0.3 in both cases. In contrast, Ren et al. [10] reported R^2 values of 0.9 and 0.7 for the anterior and lateral components, respectively. Karatsidis et al. [11] also showed higher R^2 values, with 0.9 in the anterior and 0.8 in the lateral components. Ren et al. and Karatsidis et al. likely benefit from more complex sensor configurations or computational methods, which could account for their higher correlation coefficients in these planes. While our method is robust for estimating vertical GRFs, it may require more work to improve its accuracy in the anterior and lateral planes.

The feasibility of real-time estimation of GRFs using IMUs is currently limited, primarily due to difficulties associated with processing the signal to effectively remove noise. The noise can be seen in **Figures 7** and **8** – on the Z axis at 50% of the cycle, can considerably distort the data and undermine its reliability. It may arise from an improper coupling of the IMU to the pelvis. Noise on the X axis from **Figures 5** and **6** may arise from impact impulse and improper coupling.

Improper coupling can occur due to several factors, most notably due to the process of securing the IMU to the subject which leaves room for human error. This can include incorrect positioning, and insufficient securing leading to movement of the IMU during gait. Soft tissue artifacts are also impacting the accuracy of estimating GRFs.

These issues present significant challenges for real-time GRF estimation. Without effective signal processing to eliminate these peaks and mitigate the effects of improper coupling, the use of IMUs for this purpose may deliver data that lack the necessary accuracy for dependable biomechanical analysis.

By manually selecting appropriate thresholds for HS detection, we expected our method to deliver good accuracy in estimation. However, the HS detector may fail to detect HS accurately due to suboptimal threshold optimization. As each subject has a specific walking pattern and furthermore, not all steps are identical; finding one formula to detect all HS is hard. This failure to identify the HS leads to inaccuracies when splitting the total estimated GRF into left and right GRF. Fine-tuning the threshold for detecting HS is crucial for improving the accuracy of this method, as the automatically detected thresholds aren't reliable. Further investigation could involve the use of advanced artificial intelligence (AI) and machine learning (ML) techniques to address these challenges. ML algorithms could be trained to recognize and adapt to individual gait patterns, providing a more personalized and accurate HS detection. By feeding a deep-learning neural network large amounts of data from various walking patterns, they can learn to recognize the HS of individual gaits [23]. This could potentially allow for the automatic and dynamic adjustment of thresholds for each individual and each step, thereby significantly improving HS detection.

However, while these AI-based methods could potentially improve the accuracy of HS detection and, consequently, GRF estimation, they would require substantial amounts of data and significant computational resources.

Apart from AI and ML techniques, there are several alternative automatic approaches that could be considered for improved gait pattern recognition and accurate HS detection. For instance, using the polar radius extracted from the phase portraits produced from the IMU-measured thigh angular position and velocity [24] could be employed to identify gait parameters, which could then be utilized to predict HS and also double support duration.

Signal processing techniques, including wavelet analysis [25], might also be beneficial. These methods can help identify and extract important features from the gait data, potentially improving the accuracy of HS detection. Moreover, the use of adaptive thresholding methods that adjust the detection thresholds based on the gait parameters

of an individual could be explored. This method avoids the need for manual selection and could provide a more personalized and precise HS detection.

While traditional methods or signal processing methods might not possess the complex algorithms and learning abilities that make AI and ML models 'advanced', these traditional techniques can still potentially offer an effective solution for enhancing HS detection and understanding individual gait patterns. The term 'advanced' here refers to the capacity of AI and ML models to continuously evolve and improve their performance as they process new data. This constant learning and adaptability is a distinctive feature of AI and ML models, making them highly suitable for tasks where change and adaptability are essential. However, in scenarios where implementing AI or ML might not be practicable or preferred, these more traditional methods could serve as robust alternatives.

A more approachable solution in terms of cost-effectiveness and simplicity, would be the utilization of a system comprising force-sensitive resistors (FSR). Placing FSRs on the heel and toe regions of both feet would enable accurate detection of HS and TO events. This approach eliminates the need for foot IMUs and can potentially reduce the overall cost of the system. The feasibility and effectiveness of this approach should be further investigated, taking into account the specific requirements of the system, such as the need for joint angle information.

By simplifying the measurement process and reducing the costs associated with conventional methods, our work paves the way for more accessible and affordable biomechanical analysis. Our method is not without limitations. There are challenges associated with the limited real-time processing of signals to improve estimation accuracy. The accuracy of estimating GRFs, particularly at lower speeds poses difficulties, and for shear forces further processing is needed. The incorporation of advanced signal processing techniques and algorithmic optimizations may help to overcome these challenges, thus investigating how to mitigate the “offline” processing integration in biomechanical analysis might yield better results.

5. Conclusion

In conclusion, this research contributes to the field of biomechanics, specifically in estimating GRFs with a minimal setup using three IMUs. Our strongest performance lies in the vertical component of GRFs, comparable to more complex state of the art methods. However, those considering the application of our method should be cautious of its current limitations. Most important, the method is less accurate in the anterior and lateral components, where our system needs improvements for more robust gait analysis. Furthermore, our method is best suited for conditions where the CWSA can be maintained. The assumption may not fully capture the complexities of gait in real-world scenarios where walking speed varies, potentially limiting the method's applicability in those cases.

The implications of our work span across various domains. For instance, our method could be implemented in sports science for performance analysis, in clinical settings for gait analysis in rehabilitation, and in the design and optimization of assistive devices for individuals with mobility impairments. Future work can aim to improve the accuracy of the method by integrating advanced AI techniques or cost-effective FSR. By harnessing the power of machine learning and deep learning, the system could learn to adapt to individual gait patterns, providing more personalized and accurate estimations of GRFs.

References

[1] M. H. Schwartz and A. Rozumalski, "The Gait Deviation Index: a new comprehensive index of gait pathology," Gait Posture, vol. 28, no. 3, pp. 351-357, Oct. 2008.

[2] G. Z. Yang et al., "Wearable and Implantable Sensors, Smart Implants and Virtual Reality for Digital Health Care," IEEE Trans. Biomed. Eng., vol. 68, no. 1, pp. 45-57, 2021.

[3] A. M. Sabatini, "Estimating three-dimensional orientation of human body parts by inertial/magnetic sensing," Sensors, vol. 11, no. 2, pp. 1489-1525, 2011.

[4] D. A. Winter, Biomechanical Analysis of Human Movement with Applications in Rehabilitation, 2nd ed. Hoboken, NJ: John Wiley & Sons, Inc, 1990.

[5] B. L. Scheltinga, J. N. Kok, J. H. Buurke, and J. Reenalda, "Estimating 3D ground reaction forces in running using three inertial measurement units," 2023.

[6] B. M. Nigg, R. W. De Boer, and V. Fisher, "A kinematic comparison of overground and treadmill running," Med. Sci. Sports Exerc., vol. 27, pp. 98–105, 1995.

[7] A. Forner Cordero, H. J. F. M. Koopman, and F. C. T. van der Helm, "Use of pressure insoles to calculate the complete ground reaction forces," J. Biomech., vol. 37, pp. 1427-1432, 2004.

[8] M. M. Diraneyya, J. Ryu, E. Abdel-Rahman, and C. T. Haas, “Inertial Motion Capture-Based Whole-Body Inverse Dynamics,” Sensors (Basel), vol. 21, no. 21, p. 7353, Nov. 2021.

[9] A. M. Sabatini, “Estimating Three-Dimensional Orientation of Human Body Parts by Inertial/Magnetic Sensing,” Sensors, vol. 11, no. 2, pp. 1489-1525, 2011.

[10] L. Ren, R. K. Jones, and D. Howard, "Whole body inverse dynamics over a complete gait cycle based only on measured kinematics," J. Biomech., vol. 41, no. 12, pp. 2750-2759, 2008.

[11] Karatsidis, A., Bellusci, G., Schepers, H., de Zee, M., Andersen, M., & Veltink, P. “Estimation of Ground Reaction Forces and Moments During Gait Using Only Inertial Motion Capture.” Sensors, vol. 17, no. 12, pp. 75, 2016. doi:10.3390/s17010075

[12] Yang, E. C.-Y., & Mao, M.-H. “3D analysis system for estimating intersegmental forces and moments exerted on human lower limbs during walking motion.” Measurement, vol. 73, pp. 171–179, 2015.

[13] Aurbach, M., Wagner, K., Süß, F., & Dendorfer, S.. “Implementation and Validation of Human Kinematics

Measured Using IMUs for Musculoskeletal Simulations by the Evaluation of Joint Reaction Forces." CMBEBIH, pp. 205–211, 2017. doi:10.1007/978-981-10-4166-2_31

[14] A. Ancillao, S. Tedesco, J. Barton, and B. O'Flynn, "Indirect Measurement of Ground Reaction Forces and Moments by Means of Wearable Inertial Sensors: A Systematic Review," Sensors, vol. 18, no. 8, p. 2564, 2018.

[15] J. Reh, G. Schmitz, T. H. Hwang, and A. O. Effenberg, "Acoustic Feedback in Gait Rehabilitation—Pre-Post Effects in Patients With Unilateral Hip Arthroplasty," Front. Sports Act. Living, vol. 3, 2021.

[16] S. Bonnet, C. Bassompierre, C. Godin, S. Lesecq, and A. Barraud, "Calibration methods for inertial and magnetic sensors," Sensors Actuators, A: Phys., vol. 156, no. 2, pp. 302–311, 2009.

[17] M. I. M. Refai, B. -J. F. van Beijnum, J. H. Buurke, and P. H. Veltink, "Portable Gait Lab: Estimating 3D GRF Using a Pelvis IMU in a Foot IMU Defined Frame," IEEE Trans. Neural Syst. Rehabil. Eng., vol. 28, no. 6, pp. 1308-1316, Jun. 2020.

[18] "Bionic Legs Innovations for Amputees," Living with Amplitude, Jul. 15, 2023. [Online]. Available: https://livingwithamplitude.com/bionic-legs-innovations-prosthetics-amputees/

[19] R. B. Davis, S. Õunpuu, D. Tyburski, and J. R. Gage, "A gait analysis data collection and reduction technique," Human Movement Science, vol. 10, no. 5, pp. 575-587, 1991.

[20] S. R. Donahue and M. E. Hahn, "Estimation of ground reaction force waveforms during fixed pace running outside the laboratory," Frontiers in Sports and Active Living, vol. 5, 2023.

[21] "MATLAB Function Reference," Northwestern University, Jul. 12, 2023. [Online]. Available: http://www.ece.northwestern.edu/local-apps/matlabhelp/techdoc/ref/corrcoef.html#:~:text=Each%20p%2Dvalue%20is%20the,i%2Cj)%20is%20significant.

[22] M. Yavuz, G. Botek, and B. L. Davis, "Plantar shear stress distributions: comparing actual and predicted frictional forces at the foot-ground interface," J. Biomech., vol. 40, no. 13, pp. 3045-3049, 2007.

[23] A. Parashar, A. Parashar, W. Ding, et al., "Deep learning pipelines for recognition of gait biometrics with covariates: a comprehensive review," Artif. Intell. Rev., vol. 56, pp. 8889–8953, 2023. Available: https://doi.org/10.1007/s10462-022-10365-4.

[24] Arumukhom Revi, D.; De Rossi, S.M.M.;Walsh, C.J.; Awad, L.N. "Estimation ofWalking Speed and Its Spatiotemporal Determinants Using a Single Inertial Sensor Worn on the Thigh: From Healthy to HemipareticWalking." Sensors, vol. 21, 6976, 2021.

[25] Ji, N.; Zhou, H.; Guo, K.; Samuel, O.W.; Huang, Z.; Xu, L.; Li, G. Appropriate Mother Wavelets for Continuous Gait Event Detection Based on Time-Frequency Analysis for Hemiplegic and Healthy Individuals. Sensors, vol 19, 3462, 2019.